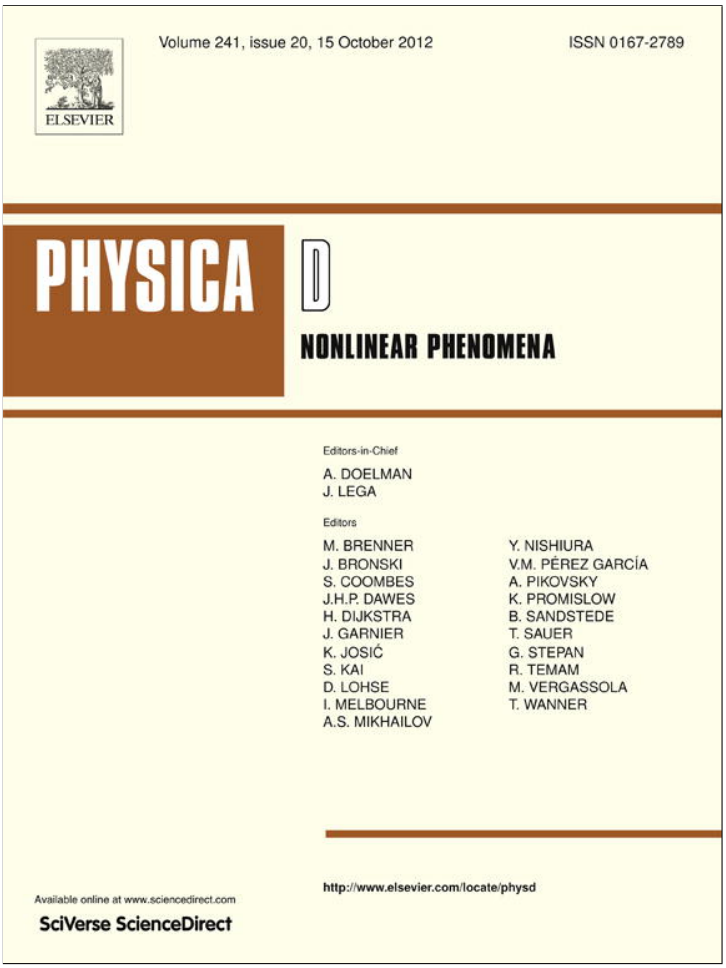

Physica D 241 (2012) 1671–1679

Contents lists available at SciVerse ScienceDirect

Physica D

journal homepage: www.elsevier.com/locate/physd

Transition to spatiotemporal chaos via stationary branching shocks and holes

Jonathan A. Sherratt [a,*], Matthew J. Smith [b]

[a] Department of Mathematics and Maxwell Institute for Mathematical Sciences, Heriot-Watt University, Edinburgh EH14 4AS, UK

[b] Computational Science Laboratory, Microsoft Research, 7 J.J. Thompson Avenue, Cambridge CB3 0FB, UK

ARTICLE INFO

Article history:
Received 25 January 2011
Received in revised form
8 June 2012
Accepted 11 June 2012
Available online 26 June 2012
Communicated by B. Sandstede

Keywords:
Turbulence
Wavetrain
Periodic travelling wave
Bifurcation
Lambda-omega
Nozaki-Bekki hole

ABSTRACT

Spatiotemporal chaos in the complex Ginzburg–Landau equation is known to be associated with a rapid increase in the density of defects, which are isolated points at which the solution amplitude is zero and the phase is undefined. Recently there have been significant advances in understanding the details and interactions of defects and other coherent structures, and in the theory of convective and absolute stability. In this paper, the authors exploit both of these advances to update and clarify the onset of spatiotemporal chaos in the particular case of the complex Ginzburg–Landau equation with zero linear dispersion. They show that very slow increases in the coefficient of nonlinear dispersion cause a shock–hole (defect) pair to develop in the midst of a uniform expanse of plane wave. This is followed by a cascade of splittings of holes into shock–hole–shock triplets, culminating in spatiotemporal chaos at a parameter value that matches the change in absolute stability of the plane wave. The authors demonstrate a close correspondence between the splitting events and theoretical predictions, based on the theory of absolute stability. They also use measures based on power spectra and spatial correlations to show that when the plane wave is convectively unstable, chaos is restricted to localised regions, whereas it is extensive when the plane wave is absolutely unstable.

1. Introduction

Many spatially extended physical systems exhibit chaotic dynamics. One model in which such spatiotemporal chaos has been studied in detail is the (cubic) complex Ginzburg–Landau equation (CGLE), which arises as the amplitude equation near a standard supercritical Hopf bifurcation, and which has been applied effectively to a wide range of physical, chemical and biological systems [1,2]. In one space dimension, two different regimes of spatiotemporal chaos occur in the CGLE. In "phase chaos" the solution amplitude is bounded away from zero, so that there is long-range phase coherence, and the phase difference across the whole domain is constant [2–5]. By contrast, "defect chaos" is characterised by large oscillations in amplitude, including isolated points ("defects") at which the amplitude is zero. At such points the phase is not defined, destroying conservation of the overall phase difference [6–8]. Changes in parameter values from the phase chaos to defect chaos regimes are characterised by a rapid increase in the density of defects [7,9,10]; in some cases there is an overlap region ("bichaos") in which there is hysteresis in the defect density.

The last few years have seen two major advances that are relevant to these considerations. Firstly there has been significant progress in understanding of the details and interaction of coherent structures, including defects, in the CGLE and other spatially extended systems [11–14]. Secondly, the theory of convective and absolute stability has been placed on a firm and more accessible footing [15–19]. In this paper we exploit both of these advances to update and clarify the onset of spatiotemporal chaos in the particular case of the CGLE with zero linear dispersion.

The equation that we study is

$$\partial A/\partial t = \partial^2 A/\partial x^2 + A - (1+ic)|A|^2 A \tag{1}$$

where the complex field A is a function of space x and time t, and $c > 0$ is the real valued control parameter. Plane waves are a fundamental solution form for (1), with the general form $A = \sqrt{1-Q^2}e^{iQx-i\omega t}$, where $\omega = c(1-Q^2)$ and $-1 < Q < 1$.

In this study we investigated the dynamics emerging in simulations of (1) under the separated boundary conditions

$$A = 0 \quad \text{at } x = 0, \qquad \partial_x A = 0 \quad \text{at } x = L, \tag{2}$$

for a suitably large domain length L and random initial conditions other than at the boundaries (detailed below). These conditions have been used in the past to investigate the generation of plane waves in real systems such as oscillatory chemical reactions and ecological systems [20–23]. Under these boundary conditions, when $c < 1.110$, perturbations to $A \equiv 0$ evolve to a solution

* Corresponding author. Tel.: +44 131 451 3249; fax: +44 131 451 3249.
E-mail addresses: J.A.Sherratt@hw.ac.uk, jas@ma.hw.ac.uk (J.A. Sherratt), Matthew.Smith@microsoft.com (M.J. Smith).

0167-2789/$ – see front matter © 2012 Elsevier B.V. All rights reserved.
doi:10.1016/j.physd.2012.06.003

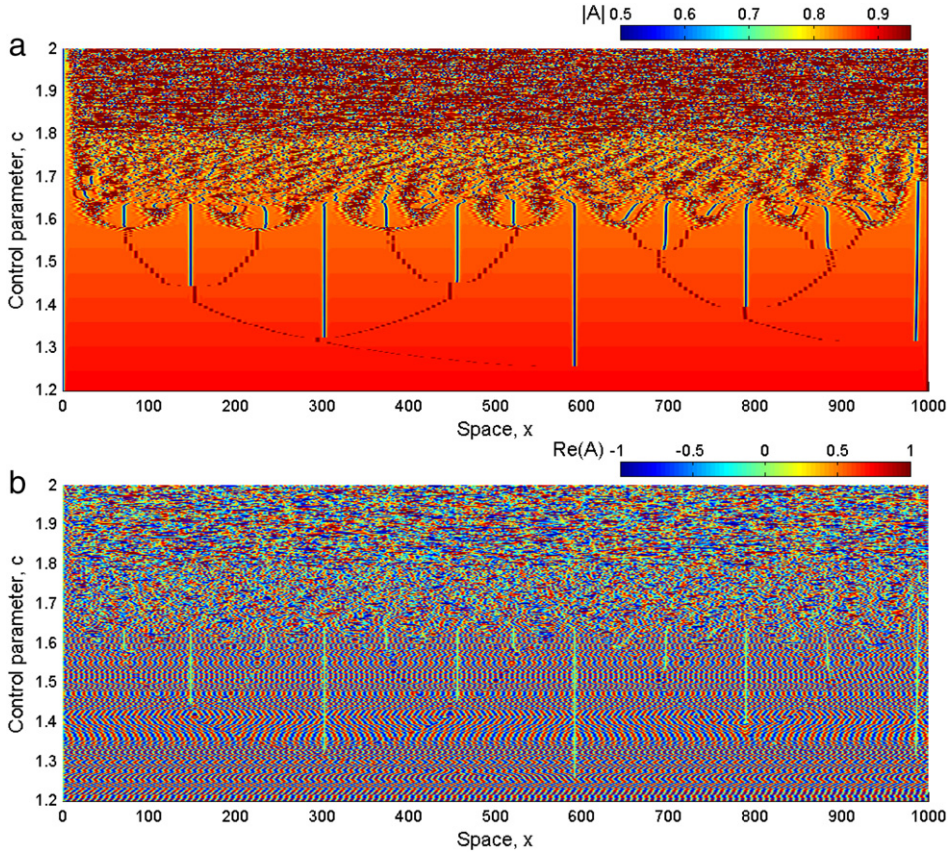

Fig. 1. (a) In this single simulation of (1), a gradual increase in the control parameter c causes a progression from an effectively uniform state in $|A|$ (a plane wave in the real and imaginary parts of A, as is shown for Re A in (b)) at $c = 1.2$ to full spatiotemporal chaos at $c = 2$. This figure combines the spatial profiles of $|A|$ immediately prior to each increment in c (each increment was 0.001, and increments were made every 3000 time units). Note that values of $|A| \leq 0.5$ are shown in the same colour; this aids visual clarity, since the regions in which $|A| < 0.5$ are very localised in space. See Fig. 2 for alternative view of this data, for specific values of c. (b) Exactly the same simulation as in (a) but instead showing Re A. This simulation took 10 days on an Intel Xenon X5560, 1333 MHz processor, with a 64 bit operating system.

that consists of half of a stationary Nozaki–Bekki hole [24,25], together with a thin boundary layer near $x = L$. When the linear dispersion parameter in the CGLE is zero, the (unique) stationary Nozaki–Bekki hole has a very simple analytical form: $|A| = |A^*| \tanh(x/\sqrt{2})$, $\partial_x \arg A = \sqrt{1-|A^*|^2} \tanh(x/\sqrt{2})$, where $|A^*(c)| = ([1+\sqrt{1+(8/9)c^2}]/2)^{-1/2}$ [22,24]. There is very close agreement between this formula and the numerical solutions of (1) and (2), for $c < 1.110$. Thus the solution is approximately constant in $|A^*(c)|$ and $\partial_x \arg(A^*(c))$, other than very close to the boundaries. In fact, both the real and imaginary parts of $A^*(c)$ exhibit plane waves:

$$A^* = |A^*| \cos(\Phi(x,t)) + i|A^*| \sin(\Phi(x,t)) \tag{3}$$

where $\Phi(x,t) = K \pm x\sqrt{1-|A^*|^2} - c|A^*|^2 t$ and K is an arbitrary constant. We refer the reader to [19,22] for details of this mechanism of plane wave generation.

Beyond $c = 1.110$, the plane waves selected by our boundary conditions are no longer stable. In a previous study we showed that when $1.110 < c < 1.576$ the instability is convective [19], meaning that small perturbations to the selected plane wave solution grow in time only while simultaneously moving. In simulations this results in bands of plane waves propagating in alternating directions, separated by localised defects known as "shocks" and "holes". In contrast, when $c > 1.576$, the selected plane waves are absolutely unstable [19], meaning that perturbations to the plane waves grow pointwise. Correspondingly, simulations show irregular spatiotemporal dynamics throughout the domain, rather than plane waves.

This study arose because we observed that when simulating (1) under separated boundary conditions, starting with various initial conditions, the dynamics emerging in simulations when $1.110 < c < 1.576$ were highly sensitive to the initial conditions, the domain length, and the value of c (an example is given in Fig. 1 of [19]). This led us to explore the effects of increasing c only, without resetting the initial conditions. Initially we increased c in relatively large increments and again found the appearance of new defect solutions at unpredictable locations. We then experimented with changing the increment size, and found that the use of sufficiently small increments in c, between time windows of sufficient length to remove transient dynamics, revealed a clear structure to the onset of spatiotemporal chaos (illustrated in Fig. 1). In this study, we therefore set out to understand this emergent structure.

Our work here extends our previous research into the spatiotemporal dynamics observed in simulations of (1) under a variety of initial and boundary conditions [14,19,27,28]. What makes this study different is that we focus on explaining one specific detailed transition to spatiotemporal chaos. In [19] we showed how to calculate the numerical threshold for absolutely unstable plane wave solutions to (1) under the same boundary conditions as studied here. In [27,28] we showed how to calculate the width of the band of plane waves emerging behind propagating fronts, a different plane wave generating mechanism, prior to their subsequent transition to spatiotemporal chaos. There, the initial perturbations to the plane wave bands were introduced by the propagating fronts.

In the scenario studied here, the perturbations to the complete solution (potentially including bands of plane waves) are introduced by the increment in the control parameter c. However, as in

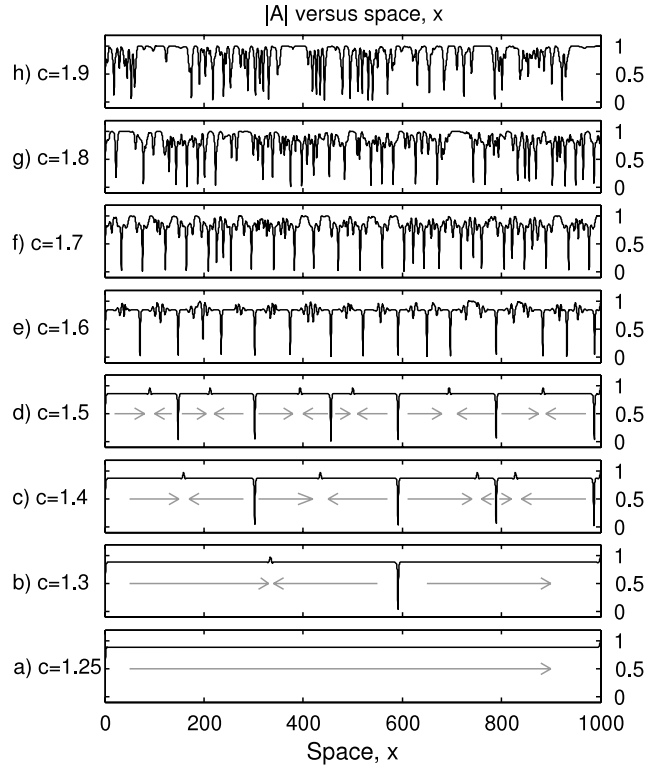

Fig. 2. The same spatial profiles as illustrated in Fig. 1a but for selected values of c. The grey arrows in a–d indicate the direction of travel of growing perturbations; these move away from holes and towards shocks when $1.110 < c < 1.576$ [25,26].

our previous studies, we show that important aspects of the spatiotemporal dynamics observed in simulations can be explained via analysis of the so-called "absolute spectrum" of the plane wave solution $A^*(c)$ in different frames of reference.

A number of previous studies have investigated the transition to spatiotemporal chaos in the CGLE [3,5,7,9,10,29–32]. Nevertheless the structured transition to spatiotemporal chaos that we report is new, to our knowledge. The key ingredients for this result are the very slow increase in the control parameter c, and the fact that our initial and boundary conditions generate a single stationary defect in the early stages of the simulation. These issues will be discussed further in Section 4.

In the next section we detail the methods we used to simulate, analyse and explain the transition to spatiotemporal chaos studied here. We then describe in detail the transition to spatiotemporal chaos observed in our simulations before extending existing mathematical theory to explain the observed transition. Finally, we discuss our results in the context of the existing literature on spatiotemporal chaos.

2. Numerical and analytical methods

2.1. Numerical simulations

To simulate (1) we converted it into two coupled partial differential equations for the real and imaginary components of A, giving

$$\partial u/\partial t = \partial u/\partial x^2 + \left(1 - |A|^2\right) u + c|A|^2 v \tag{4a}$$

$$\partial v/\partial t = \partial v/\partial x^2 + \left(1 - |A|^2\right) v - c|A|^2 u \tag{4b}$$

where $A = u + iv$ and $u, v \in (-1, 1)$. We simulated (4) with boundary conditions $A = 0$ at $x = 0$ and $\partial_x A = 0$ at $x = 1000$ using a standard semi-implicit finite difference method with a space resolution of 0.2 and a time step of 0.001. These resolutions reproduce theoretically predicted values of $A^*(c)$ to 99.9% accuracy [19] and further increases do not affect the positions or behaviour of the holes or shocks.

All of our numerical simulations began with pseudo-random initial values of u and v between 0 and 1 at each point in space (except $u = v = 0$ at $x = 0$), and $c = 1.1$. Simulations were then run until a stable plane wave solution had filled the domain (other than close to the boundaries). We then conducted a series of numerical experiments, starting with this solution as an initial condition, in which we repeatedly incremented c between sufficiently long intervals of simulation time for the transient dynamics to disappear. The length of time required for transients to disappear is dependent on c and the domain length, and can be estimated via linear stability analysis of $A^*(c)$ (described below).

The final simulation we chose for subsequent analysis was conducted on a domain length of 1000 space units in which we incremented c by 0.001 every 3000 time units. We chose this domain length as a compromise between being sufficiently large for spatiotemporal structure to emerge in the simulations and being sufficiently small to allow simulations to be completed within reasonable time frames. However, our findings are not affected by further increases in the domain size, nor by increments in c below 0.001, with one exception: the formation of the initial hole–shock pair in the interior of the domain (see details below).

2.2. Characterising spatiotemporal chaos

We used three measures to statistically characterise the spatiotemporal dynamics observed in Fig. 1: Lyapunov exponents, Fourier analysis of the time series at each space point, and the correlation between the dynamics of nearby space points. Lyapunov exponents indicate whether initially very similar spatial profiles converge or diverge through time. Divergent trajectories of initially similar states are one indicator of spatiotemporal chaos. We did not use Lyapunov exponents to characterise the spatiotemporal nature of diverging trajectories, as can be done using "convective Lyapunov exponents" [33–35]; instead we used the absolute spectrum of $A^*(c)$ for this purpose, as discussed in the next section.

To calculate Lyapunov exponents we employed the same methodology as described in [33]; solving Eq. (4) alongside the first order terms of its Taylor series expansion

$$\begin{aligned}\delta u_t &= \delta u_{xx} + \delta u(1 - 3u^2 - v^2 + 2cuv)\\ &\quad + \delta v(-2uv + cu^2 + 3cv^2)\end{aligned} \tag{5a}$$

$$\begin{aligned}\delta v_t &= \delta v_{xx} + \delta v(1 - 3v^2 - u^2 - 2cuv)\\ &\quad + \delta u(-2uv - 3cu^2 - cv^2)\end{aligned} \tag{5b}$$

where δu and δv are the perturbations to u and v respectively, and $\delta A = \delta u + i\delta v$. We selected solutions from Fig. 1 just prior to each increment in c and used them as initial conditions for simulating (4) and (5) in parallel, for fixed c. The largest Lyapunov exponent for A was then calculated as $\lim_{t\to\infty} \Lambda(A)$ where

$$\Lambda(A) = \ln \frac{\|\delta A(x,t)\|}{\|\delta A(x,0)\|} \quad \text{and}$$

$$\|\delta A(x,t)\| = \left\{\int_{x=0}^{x=L} |\delta A(x,t)|^2 dx\right\}^{1/2} \tag{6}$$

with $L = 1000$. We chose $\delta u = \delta v = 10^{-4}\zeta(x)$ as initial perturbations for all points in space, where $\zeta(x)$ is a pseudorandom number between 1 and 0, other than at $x = 0$ where $\delta u = \delta v = 0$.

We used Fourier analysis to characterise the nature of autocorrelation in time series data at each space point. A wide range

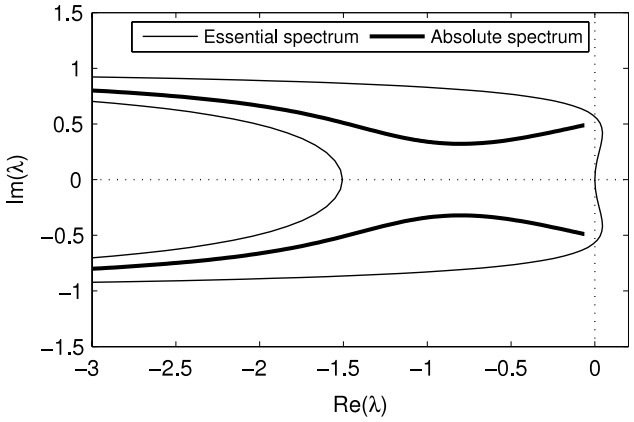

Fig. 3. An example of the essential and absolute spectra of a plane wave solution of (1). The example shown is for $c = 1.4$, with the plane wave being the asymptotic plane wave of a stationary Nozaki–Bekki hole. In this case the plane wave is unstable, but absolutely stable: the essential spectrum crosses the imaginary axis, but the absolute spectrum is confined to the left-hand half of the complex plane. The spectra were calculated using numerical continuation, following the approach described in [15,19].

of temporal frequencies is one characteristic of chaotic dynamics, and the spatial synchrony of these complex temporal dynamics can provide insight into the spatial component of the disorder. To obtain data for analysis we selected solutions from Fig. 1 just prior to each increment in c as initial conditions and simulated (4) for a further 1000 units of simulated time. We also used this data to analyse the degree of correlation between the time series of different points in space. We characterised the degree of synchrony using the Pearson product-moment correlation coefficient

$$\rho = \sum_{t=0}^{t=T} \frac{\left(|A|(x_1,t) - \left|\overline{A}\right|(x_1)\right)\left(|A|(x_2,t) - \left|\overline{A}\right|(x_2)\right)}{T\left|\widehat{A}\right|(x_1)\left|\widehat{A}\right|(x_2)} \tag{7}$$

$(-1 < \rho < 1)$ where $\left|\overline{A}\right|$ and $\left|\widehat{A}\right|$ are the mean and standard deviations of $|A|$ at space point x over T sampled time points (at intervals of 1 time point), respectively. Here $x_1 \in (100, 900)$ and $x_2 \in (x_1 - 100, x_1 + 100)$. We used $T = 1000$ for our analysis. A low degree of synchrony (ρ close to zero) between the time series of nearby points in space can be an indicator of spatiotemporal chaos. Note that correlation coefficients such as that defined in (7) have been used in many previous studies of spatiotemporal chaos (e.g. [7,9]).

2.3. Overview of mathematical theory on the way in which perturbations to the solution $A^*(c)$ grow in space and time

Denote by $\sum_L$ the spectrum of the linearisation of (1) with separated boundary conditions such as (2) about a plane wave solution. Then the "absolute spectrum" $\sum_{abs}$ is the set of accumulation points of $\sum_L$ as $L \to \infty$. The plane wave is described as "absolutely stable" if the absolute spectrum is confined to the left-hand half of the eigenvalue complex plane; this implies that there are no perturbations that grow pointwise [16]. The absolute spectrum differs from the essential spectrum because the latter corresponds to both perturbations that grow pointwise and perturbations that only grow while simultaneously moving. Thus the absolute spectrum lies to the left of the essential spectrum in the eigenvalue complex plane; this is proved formally in [36]. Fig. 3 shows an example of the two spectra. Plane waves that are unstable but absolutely stable are known as "convectively unstable". Detailed discussions of the absolute spectrum are given in [15,16,19], and examples of other approaches to determining absolute stability are described in [2,18,37].

We conducted an analysis of the absolute stability of the solution $A^*(c)$ in moving frames because it has been used previously to explain the spatiotemporal dynamics observed in simulations of (1) [19,27,38]. Our analysis here is based upon linearisation of (1) about the theoretical plane wave $A^*(c)$. This contrasts with the Lyapunov exponent, which describes the long term dynamics of small perturbations to (1) via the linearisation of the entire spatiotemporal solution to (1). Note that in the case of unstable plane waves, this spatiotemporal solution is typically not a plane wave: rather it consists either of a series of bands of plane waves separated by defects, or of spatiotemporal disorder.

Our goal is to calculate the rate of growth of small perturbations to $A^*(c)$ as a function of their velocity. We begin by rewriting (1) as two real equations for the amplitude and phase of A, and replacing the spatial coordinate x with a velocity-dependent spatial coordinate $z = x - Vt$, where V is an arbitrary reference frame velocity. This gives

$$r_t = r_{zz} + Vr_z + r(1 - r^2) - r\theta_z^2 \tag{8a}$$

$$\theta_t = \theta_{zz} + V\theta_z - cr^2 + 2r_z\theta_z/r \tag{8b}$$

where $r = |A|$ and $\theta = \arg(A)$. We then linearise these equations about the plane wave solution $A^*(c)$ (as given by (3)), which has the form $r = |A^*|$ and $\theta = -c|A^*|^2 t \pm x\sqrt{1 - |A^*|^2}$ $(0 \le |A^*| \le 1)$. To leading order, linear perturbations $\delta r(x,t)$ and $\delta\theta(x,t)$ of this solution satisfy

$$\delta r_t = \delta r_{zz} + V\delta r_z - 2|A^*|^2\delta r - 2|A^*|\delta\theta_z\sqrt{1 - |A^*|^2}$$

$$\delta\theta_t = \delta\theta_{zz} + V\delta\theta_z - 2c|A^*|\delta r + 2\delta r_z\sqrt{1 - |A^*|^2}/|A^*|.$$

In the standard way, we look for solutions of the form $(\delta r, \delta\theta) = (\bar{r}, \bar{\theta})e^{\lambda t + ikz}$, where $\bar{r}$ and $\bar{\theta}$ are constants, giving

$$\lambda\bar{r} = -k^2\bar{r} + Vik\bar{r} - 2|A^*|^2\bar{r} - 2ik|A^*|\bar{\theta}\sqrt{1 - |A^*|^2} \tag{9a}$$

$$\lambda\bar{\theta} = -k^2\bar{\theta} + Vik\bar{\theta} - 2c|A^*|\bar{r} + 2ik\bar{r}\sqrt{1 - |A^*|^2}/|A^*|. \tag{9b}$$

The dispersion relation for non-trivial solutions of these linear equations is quadratic in the temporal eigenvalue λ and quartic in the spatial frequency k. Therefore, for each λ there are four associated values of k which we denote by $k_1, \ldots, k_4$ with $\mathrm{Im}\,k_1 \le \mathrm{Im}\,k_2 \le \mathrm{Im}\,k_3 \le \mathrm{Im}\,k_4$. To calculate absolute stability for a given reference frame velocity V we then need to calculate the λ values associated with so-called "branch points" in the absolute spectrum [15,19], which are values of λ for which $k_2 = k_3$. These points give the maximum growth rates of perturbations to $A^*(c)$ moving with velocity V [27], and we denote the corresponding values of λ and $k_2 = k_3$ by $\lambda_{\max}(V)$ and $k_{\max}(V)$.

In summary, in order to calculate the maximum growth rates of perturbations to $A^*(c)$ we solved (9) for a given c, for a range of reference frame velocities V, allowing us to calculate the spatiotemporal dynamics of perturbations in the plane wave. We used these calculations of the growth rates and velocities of small perturbations to $A^*(c)$ to investigate the widths of the bands of plane waves between the shock and hole solutions when $1.110 < c < 1.576$. In the next section we give an overview of the computational methods we used to perform these calculations.

2.4. Numerical continuation of the absolute spectrum of $A^*(c)$

Calculation of the entire absolute spectrum can be done by numerical continuation of (9). An initial solution is required for this continuation, and this can be obtained by numerical solution of the dispersion relation for fixed c and V. Full details of the calculation are given in [19]. In fact, for our purposes it is sufficient to determine the most unstable points in the absolute spectrum, which for (1) are branch points [19]. To calculate these, one eliminates λ from the dispersion relation and its derivative with

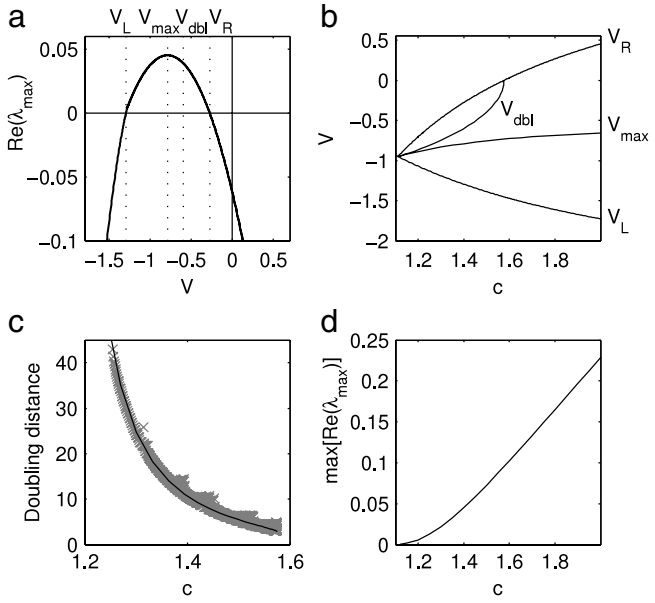

Fig. 4. Key components of our analysis of the growth rate of perturbations to $A^*(c)$. (a) A typical example of the relationship between co-moving frame velocity, V and the real part of the growth rate of perturbations to the plane wave $A^*(c)$, $\mathrm{Re}\,\lambda_{\max}$; here $c = 1.4$. (b) Relationship between c and significant points on the $V - \mathrm{Re}\,\lambda_{\max}$ curve indicated in (a). Note that the V_{dbl} and V_R curves intersect at $c = 1.576$, which is the onset of absolute stability; at that point $V_{dbl} = V_R = 0$. (c) The black line shows the relationship between c and the "doubling distance". The grey crosses are our measured widths of plane wave bands in Fig. 1, rescaled using the grey regression line in Fig. 8. (d) Maximum growth rate of travelling perturbations to the plane wave $|A^*|$ for different values of c: this is the maximum value of $\mathrm{Re}\,\lambda_{\max}$ for $V_L < V < V_R$.

respect to k, giving a fourth order polynomial in k. One then back-substitutes each of the roots for k to find the associated values of λ and hence the other two (non-repeated) roots for k of the dispersion relation. From this, one can determine whether it is k_2 and k_3 that are the repeated roots, as required for a branch point (see above). A fuller discussion of this approach is given in [19]. As an aside, we mention that the fact that the most unstable points in the absolute spectrum are branch points is a special property of the CGLE with zero linear dispersion, and does not hold for some non-zero linear dispersion coefficients (see [15] for an example).

2.5. Definition and calculation of the "doubling distance"

For all $c \in (1.110, 1.576)$, we find that $\mathrm{Re}\,\lambda_{\max}(V)$ has a unique maximum at which it is positive, and roots V_L and V_R, where $V_L < V_R < 0$ (illustrated in Fig. 4a, b). (A negative velocity corresponds to a direction of travel from the holes towards the shocks in our simulations.) This implies that for any velocity V between V_L and V_R, there is a linear mode that travels with velocity V whilst growing, but there are no growing modes for $V < V_L$ or $V > V_R$. At $c = 1.576$, which is the onset of absolute instability, $V_R = 0$; this corresponds to the onset of stationary growing linear modes.

We make the reasonable assumption that an increment in c applies a perturbation containing all unstable linear modes at all points in the interior of the domain. For $c \in (1.110, 1.576)$, these modes travel while simultaneously growing. For any given velocity of travel V, a mode will first double in size after travelling a distance $\log(2)V/\mathrm{Re}\,\lambda_{\max}(V)$; here "size" refers to the amplitude of the perturbation in A. We have shown previously [27] that the velocity $V = V_{dbl}$ at which this distance is minimised is given by $V_{dbl}[\mathrm{Im}\,(k_{\max}(V_{dbl}))] + \mathrm{Re}\,[\lambda_{\max}(V_{dbl})] = 0$. Note that V_{dbl} is different from $V_{\max}$ (Fig. 4a), the reference frame velocity that maximises $\mathrm{Re}\,\lambda_{\max}(V)$; $V_{\max}$ itself has no particular significance for our calculations.

We define the "doubling distance" as the shortest distance travelled by a perturbation to $A^*(c)$ before it doubles in size. This is given by $|\log(2)V_{dbl}/\mathrm{Re}\,\lambda(V_{dbl})| = |\log(2)/\mathrm{Im}\,(k_{\max}(V_{dbl}))|$ [27] (see Fig. 4b for an example of V_{dbl} plotted against c and Fig. 4c for the relationship between c and the doubling distance that was used in Fig. 8). Shifts in the positions of shock solutions, and the formation of new shock–hole–shock triplets, both occur in response to the perturbations arising from incrementing c. Specifically, both behaviours occur when linear modes in these perturbations grow to (different) critical sizes, and hence in both cases the wider of the two adjacent regions of plane waves is proportional to the doubling distance.

3. Results

3.1. Dynamics observed in numerical simulations

The transition we studied to spatiotemporal chaos is illustrated in Fig. 1. At sufficiently low values of c the spatial profile of $|A|$ is approximately constant away from the boundaries (Fig. 1a), with the real and imaginary parts of A exhibiting plane waves (Fig. 1b). This corresponds to the solution $A = A^*(c)$, as described above. However, at $c = 1.255$, two defects form within the domain, a "shock" and a "hole", in which $|A|$ is noticeably higher and lower than the surrounding solution, respectively [2]. Further numerical experiments with smaller increments in c revealed that the value of c at which this initial shock–hole formation event occurs is sensitive to the size of the increment in c.

After the initiation of the first shock–hole pair we observe a progression of diverging neighbouring shocks and holes, interspersed with the splitting of shock solutions into new shock–hole–shock triplets. At around $c = 1.576$, the shocks are replaced by regions exhibiting irregular spatiotemporal dynamics, although the holes persist in roughly evenly spaced locations until approximately $c = 1.9$, after which recognisable spatial structures disappear (Figs. 1 and 5a, b).

Our analyses of the spatiotemporal dynamics at each c value confirmed that the appearance of spatiotemporal chaos coincides with the onset of absolute instability of the plane wave solutions at $c = 1.576$. When $c < 1.255$, prior to the onset of hole–shock pairs in the domain, the largest Lyapunov exponent is zero (Fig. 6b). Further analysis reveals that the perturbations are ultimately all convected towards the right hand boundary where they are absorbed, although this leaves a permanent phase shift in A such that $\|\delta A(x, t)\|$ asymptotically approaches a constant through time (Fig. 6a). When $1.255 < c < 1.576$ the largest Lyapunov exponents are also zero (Fig. 6b). Again the perturbations lead to a permanent change in the phase of A (Fig. 6a). However, in these cases the perturbations are convected towards their neighbouring hole solutions before eventually being absorbed. When $c > 1.576$ the largest Lyapunov exponent is positive (Fig. 6b). In these cases the initial perturbations increase in size through time at all points in space (Fig. 6a, b).

Our other statistical analyses of the time series data indicate that spatiotemporal chaos is initially spatially localised at $c = 1.576$, eventually becoming spatially delocalised for sufficiently large values of c. For example, Fig. 5 illustrates spatially localised chaos when $c = 1.6$ (at around $x = 750$ and $x = 850$), and spatially delocalised chaos when $c = 1.9$. Fourier analysis of the temporal data indicates that when $c = 1.9$, a wide spectra of multiple frequencies occurs throughout space—this is one characteristic of chaotic dynamics (Fig. 5d). However it only occurs in localised regions when $c = 1.6$ (Fig. 5c); elsewhere the temporal dynamics are periodic, with a dominant frequency of around 0.1. Another characteristic of spatiotemporal chaos is the rapid loss of correlation in the temporal dynamics of neighbouring

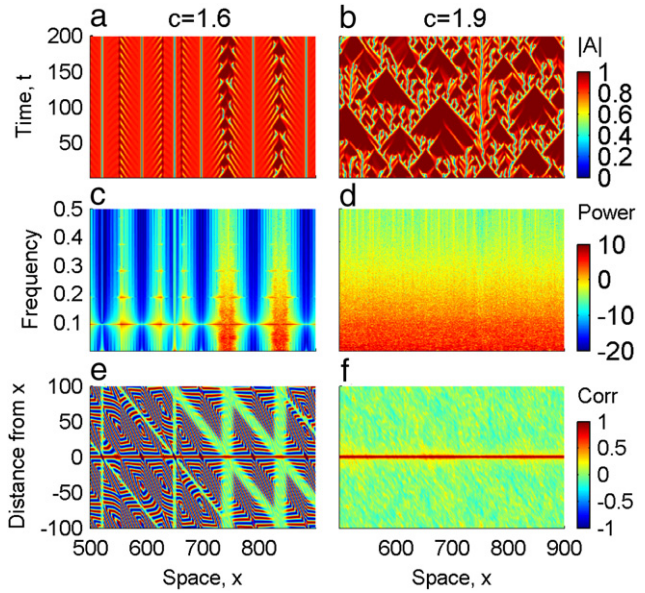

Fig. 5. Spatiotemporal chaos in $|A|$ changes from spatially localised to global as the control parameter c is increased from $c = 1.6$ to $c = 1.9$. (a) and (b), respectively, illustrate the contrasting dynamics at these extremes. For clarity we only show a sub-region of space ($500 < x < 900$). (c), (d) Log power spectrum (Power) of the discrete Fourier transform of the time series of $|A|$ for each space point. (e), (f) The correlation (Pearson correlation coefficient: Corr) between the dynamics in $|A|$ at each point in space (horizontal axis) and that of neighbouring points within 100 space units proximity (vertical axis).

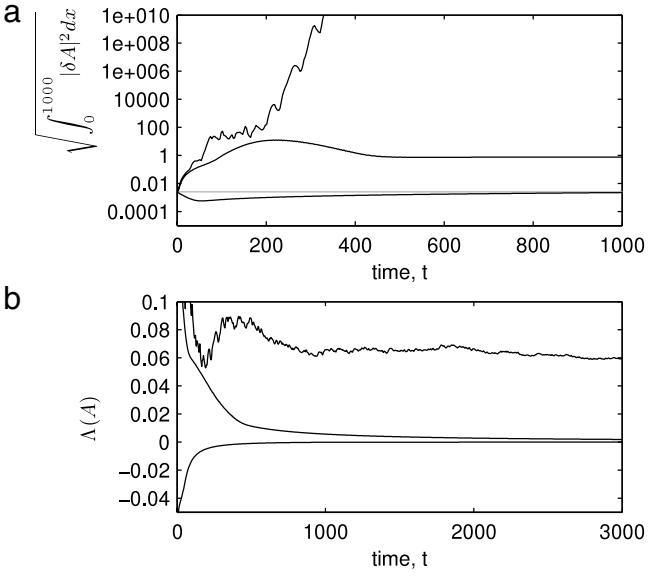

Fig. 6. Details of our analysis of the largest Lyapunov exponents for the dynamics in Fig. 1. (a) Integrals of the perturbation sizes δA, $\|\delta A(x,t)\|$, defined in Eq. (6), across space through time (black lines) for $c = 1.1$, $c = 1.5$ and $c = 1.6$ (bottom, middle and top lines, respectively). The grey line indicates $\|\delta A(x,t)\|$ at $t = 0$ when $c = 1.1$ ($\|\delta A(x,t)\|$ is similar for the other values of c at $t = 0$). (b) Estimation of $\Lambda(A)$ through time (black lines) for $c = 1.1$, $c = 1.5$ and $c = 1.6$ (bottom, middle and top lines, respectively), according to Eq. (6). The largest Lyapunov exponent is $\lim_{t\to\infty} \Lambda(A)$.

space points with increasing separation. When $c = 1.9$, this occurs at every point in space; this is indicated by the homogeneous grey (green online) shading away from "Distance from x" $= 0$ in Fig. 5f. (Fig. 5f). However, when $c = 1.6$, it only occurs in localised regions, namely the wide grey (green online) vertical lines centred on $x \approx 740$ and $x \approx 840$ in Fig. 5e. Elsewhere the correlation oscillates between high positive and high negative values as separation is

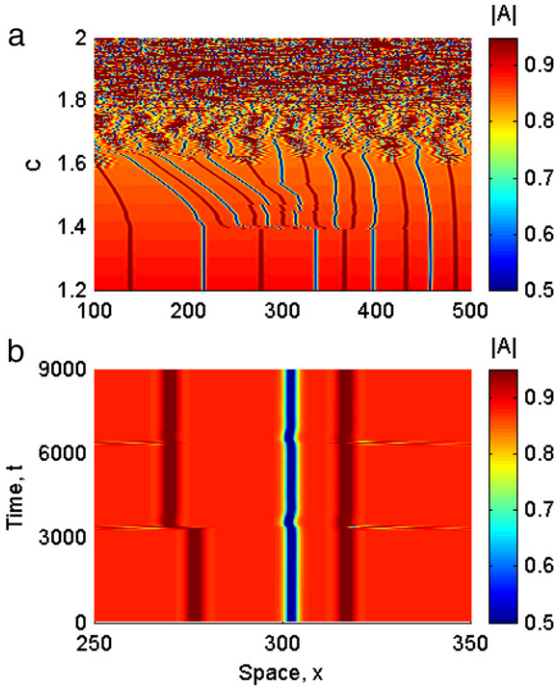

Fig. 7. The formation of shock–hole solutions is subcritical. (a) If we repeat the study illustrated in Fig. 1 but instead start at $c = 2$ and decrease c by 0.001 every 3000 time units then shock and hole solutions persist down to $c = 1.2$. Note that the direction of increasing time is down the page in this figure and up the page in Fig. 1. For clarity we only show a sub-region of space. (b) We took the solution from Fig. 1 immediately after the first shock–hole–shock triplet had formed at $c = 1.324$, located around $x = 300$ in Fig. 1. We ran this for a further 3000 time units, then decreased c by 0.001, ran for a further 3000 time units, then decreased c by 0.001 again. The shock–hole–shock triplet persists throughout the simulation. Again, for clarity we only show a sub-region of space. In both (a) and (b), values of $|A| \leq 0.5$ are shown in the same colour; this aids visual clarity, since the regions in which $|A| < 0.5$ are very localised in space.

increased, other than when the neighbouring point lies in a chaotic band (the wide grey (green online) diagonals in Fig. 5e).

3.2. Details of the transition to spatiotemporal chaos

When $1.110 < c < 1.576$ the solution $A = A^*(c)$ is convectively unstable [19], meaning that small perturbations to the plane wave $A^*(c)$, introduced by the small increment in c, grow in time only while simultaneously moving. When $c < 1.255$, these perturbations all travel from left to right and are eventually absorbed by the right-hand boundary. Our results suggest that the defect solutions form at $c = 1.255$ because the perturbations caused by the increment in c become large enough to induce the formation of a shock–hole pair in the interior of the domain. Further simulations reveal that this transition is subcritical: if we terminate the increase in c after initial defect formation and instead begin to gradually decrease c then the shock–hole pairs persist. Similar studies show that, beyond $c = 1.255$, the branching of shocks into shock–hole–shock triplets is also subcritical (Fig. 7).

When $1.110 < c < 1.576$, perturbations always travel away from the holes and towards the shocks, as illustrated in Fig. 2a–d. Our perturbation analyses revealed that shocks move to a new position when they receive perturbations above a critical size: smaller perturbations are absorbed. They actually move via discrete jumps because shock–hole separations are restricted to a discrete family of possible values [14]. Perturbations travelling through larger bands of plane waves reach the critical size at lower values of c than those travelling through smaller

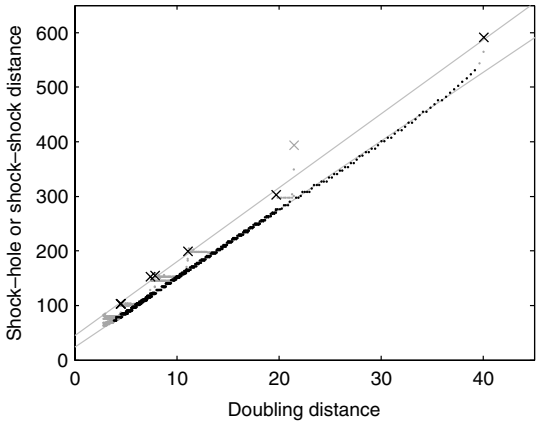

Fig. 8. The distance between a shock and the furthest adjacent hole (black points) correlates tightly with the doubling distance (grey regression line through the black points; $r^2 > 0.999$). Similarly, the distance between the furthest adjacent hole and the point at which a shock splits into a shock–hole–shock triplet (black crosses) also correlates tightly with the doubling distance (grey regression line through the black crosses; $r^2 > 0.999$). Our regression analysis excludes explicable outliers (grey points/crosses). These fall into several categories. (i) A shock is equidistant from the neighbouring holes (see main text). (ii) A shock and hole solution pair forms close to the right-hand boundary, which has a stabilising effect on the adjacent plane wave. (iii) When a shock–hole pair initially forms, the new shock and hole solutions can interact weakly over relatively short distances [14], causing shocks to initially prevent the holes moving as far as predicted by our theory. However, after a few increments in c this interaction loses its relevance [14]. (iv) We also excluded results for $1.55 < c < 1.576$ because we expect our theory, based on linear stability analysis, to become less accurate close to the absolute stability boundary at $c = 1.576$ due to nonlinear effects [27].

bands of plane waves, and the width of the largest neighbouring region correlates tightly with the "doubling distance" (Fig. 8). An exception occurs when a shock is equidistant from the neighbouring holes. The shock is then pushed equally in opposite directions, and consequently does not move. However, the growth rate of the perturbations, caused by each increment in c, increases with c (see Fig. 4) and eventually they grow sufficiently large to transform the shock into a shock–hole–shock triplet. The values of c at which new hole solutions form also correlates tightly with the doubling distance (Fig. 8). These observations suggest that there are two critical sizes of perturbation: one for the movement of a shock to a new location, and another (larger) for the transformation of a shock to a shock–hole–shock triplet.

The value of c at which spatiotemporal irregularities appear within the solution ($c = 1.576$) corresponds to the theoretically predicted value of c at which perturbations to the plane wave $A^*(c)$ grow pointwise ("absolute instability" [15]). Beyond this, the shocks are replaced by more irregular regions in space, although holes persist in roughly evenly spaced locations until approximately $c = 1.9$, after which recognisable spatial structures disappear (Figs. 1 and 5a, b). Holes can persist because for $c > 1.12$ they are known to be "core stable" [39–43]. These references and other relevant results that we are aware of concern linear stability; we undertook a numerical study of nonlinear stability. This showed that for c in the range 1.6–1.9, holes are remarkably robust to perturbations (Fig. 9). Specifically, we simulated a single hole in the interior of a relatively small domain with boundary conditions $\partial_x A = 0$ at either end, and subjected it to perturbations of various sizes. When $c < 1.576$ we could extract a shock–hole–shock triplet from the simulation used to produce Fig. 1 and use this as an initial condition for these simulations. Thus we actually had half of a shock solution at each domain edge, with a hole solution in the interior of the domain. For more irregular solutions, when $c > 1.576$, we extracted the hole and its adjacent neighbouring plane wave up to the point in space where the solution became irregular in time. This judgement was made by

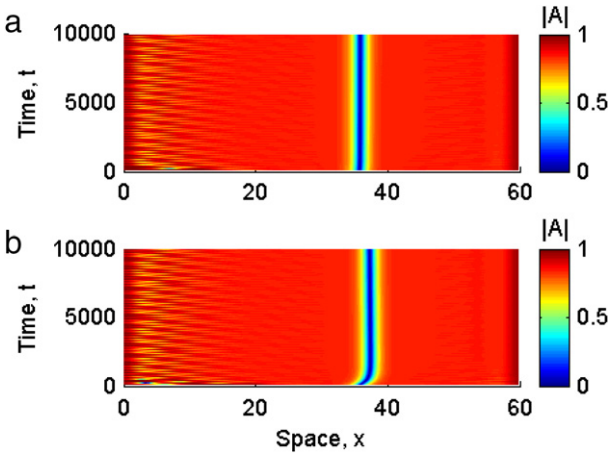

Fig. 9. Hole solutions are very robust to perturbations. Both plots show the spatiotemporal dynamics of $|A|$ when $c = 1.6$. In (a) the real and imaginary parts of A were incremented by 0.1 in the region $20 < x < 25$: this has no long term effect on the hole. In (b) an increment of 0.5 was applied to the same region in the same way; this was sufficient to move the hole solution. Not included here are the straightforward analyses we performed to verify that the simulations settled to an equilibrium state both before and after these perturbations were applied.

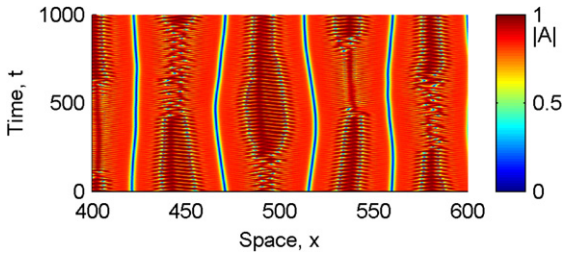

Fig. 10. Illustration of "wobbling" hole solutions. We extracted the solution from Fig. 1 for $c = 1.7$ and continued simulating (1) for a further 1000 time units. For clarity we only show a sub-region of space ($400 < x < 600$).

eye but it was reliable enough to simulate stable individual hole solutions. Extracting the initial condition in this way and then simulating under the different boundary conditions introduces a small initial perturbation. Therefore we initially solved (1) using these initial and boundary conditions for sufficient time to remove the resulting transient dynamics. We then perturbed the plane wave to one side of the hole solution, and observed the subsequent behaviour (see Fig. 9 for an example). This showed that hole solutions are very robust to perturbations.

As c increases above 1.576, holes are subjected to a progressively larger onslaught of perturbations following each increment in c; this results in a "wobbling" of the holes in which individual hole solutions persist but are visibly mobile (Fig. 10). Eventually these perturbations become sufficient to engulf the holes. However, short-lived hole-like structures remain a feature of the resulting spatiotemporal chaos [30].

4. Discussion

Our results show that the development of spatiotemporal chaos is associated with a change in absolute stability, and with an increase in the density of defects. Neither of these findings are new. The onset of absolute instability has long been known to be linked to spatiotemporal chaos, particularly in the context of hydrodynamics [44–47], and the rapid increase in defect density at the transition from phase to defect chaos in the CGLE was established 20 years ago. The essential new feature of our results is that the defects are stationary. Because of unusual symmetries, the CGLE has a one-parameter family of holes [48,49]. This family

is often parametrised by the hole velocity, which is proportional to the difference in amplitude of the two asymptotic plane waves [13,22,50]; this proportionality also applies to coherently moving shock–hole–shock triples. In our setup, new shock–hole–shock triples form within a uniform expanse of plane waves, and thus their velocity is forced to be zero. Although holes and shocks are generic features of many spatially extended oscillatory systems [26], they are in general mobile, making the onset of spatiotemporal chaos less clearly defined. Our findings imply that new insights might be gained by restricting, or controlling for, the movement of spatiotemporal solutions, such as defects. Our study also argues for experimental protocols involving slow changes in a control parameter without resetting the apparatus, allowing sufficient time for transient dynamics to elapse before the next parameter increment.

The combination of stationary defects and a very gradual change in the control parameter has enabled a detailed predictive study of shock movement and shock–hole–shock triplet formation, based on the theory of absolute and convective stability. Increasing the control parameter causes the initial background state to become increasingly unstable. Such instability is initially only convective, and sufficient convective instability leads to the formation of defects which stabilise the spatiotemporal dynamics. Our results suggest that the branching pattern of shocks and holes then arises from the interplay between convectively growing perturbations in the plane wave and the ability of shocks to absorb such perturbations, which often involves a translation in space. After the plane wave has become absolutely unstable it is then the holes that have a stabilising effect: they can continue to organise the spatiotemporal dynamics for a limited range of larger control parameter values.

The results that we have described and analysed are for boundary conditions $A = 0$ and $\partial_x A = 0$ at opposite ends of the domain. The significance of these conditions is that for low c they generate a half-hole and half-shock at the boundaries, separated by a uniform expanse of plane wave; this is independent of initial conditions. The transition to spatiotemporal chaos that we have described does occur with other boundary conditions, but it requires the specification of particular initial conditions. For example, for zero flux conditions $\partial_x A = 0$ at both boundaries, random initial conditions typically evolve to $A = 1$, corresponding to spatially homogeneous oscillations of the real and imaginary parts. However if one imposes an isolated hole at the centre of the domain, half a shock at each boundary, and the asymptotic plane wave of the hole elsewhere, the subsequent evolution as c is slowly increased mirrors exactly that shown in Fig. 1. The same applies for periodic boundary conditions, although the initial hole must be located slightly off-centre in order that $\mathrm{Re}\,A$ and $\mathrm{Im}\,A$ satisfy the required periodicity.

Spatially intermittent chaotic dynamics such as those observed in our simulations have been studied in other experimental and mathematical systems [2,29,31,51–57]. For example, studies of fluid dynamics in simple experimental systems (plane Couette flow) have generated intermittent turbulent states between regions of laminar flow for particular values of a control parameter [52,53,58,59]. These dynamics appear to be highly analogous to the intermittent chaotic regions illustrated in Figs. 5a and 10 (for example, compare these figures with Fig. 3 of [52]).

Our study raises a number of further questions about the transition to spatiotemporal chaos observed in our simulations. While we found that the initial formation of shocks and holes is sensitive to the size of increment in c, we do not understand fully this dependency, nor the mechanism by which shock–hole pairs are initiated. Moreover, our understanding of the branching pattern of shock and hole solutions is primarily based on our understanding of the spatiotemporal dynamics of small perturbations to the plane wave solution. Extending this analysis to the stability of shock solutions (and potentially also hole solutions) could enable us to explain more precisely why certain perturbations are absorbed by the shock solutions, while others result in shock displacement. Moreover, our characterisation of the growth rate of perturbations to the plane wave (e.g. Fig. 4a) appears to be highly analogous to the characterisation of small perturbations to generic spatiotemporal solutions using "convective Lyapunov exponents" (e.g. [33,35]). The basic difference between these measures is that convective Lyapunov exponents are a property of the solution as a whole, rather than just the plane waves between the shocks and holes; a natural future research direction would be to investigate in detail the relationships between the two measures. Finally, our analysis of the spatiotemporal dynamics in the region of parameter space in which plane wave solutions are absolutely unstable was limited for brevity. Further analysis is needed to explain the precise roles played by defect solutions, particularly holes, in spatially organising the spatiotemporal chaos in that parameter region.

Acknowledgements

We are extremely grateful to Jens Rademacher (CWI, Amsterdam) for many discussions which made a significant contribution to our work. We also thank Vassily Lyutsarev and Eric Hellmich (both Microsoft Research, Cambridge) for technical assistance, Tom Bridges (University of Surrey), Henrik Jensen (Imperial College, London), and Sergei Kuksin (Ecole Polytechnique, Paris) for helpful discussions and Andrew White (Heriot-Watt University), Alex Brändle, Neil Dalchau, Stephen Emmott, Greg McInerny, and Andrew Phillips (Microsoft Research, Cambridge) for advice on the manuscript. JAS was supported in part by a Leverhulme Trust Research Fellowship.

References

[1] Y. Kuramoto, Chemical Oscillations, Waves, and Turbulence, Springer-Verlag, Berlin, 1984.
[2] I.S. Aranson, L. Kramer, The world of the complex Ginzburg–Landau equation, Rev. Modern Phys. 74 (2002) 99–143.
[3] A. Torcini, Order parameter for the transition from phase to amplitude turbulence, Phys. Rev. Lett. 77 (1996) 1047–1050.
[4] A. Torcini, H. Frauenkron, P. Grassberger, Studies of phase turbulence in the one-dimensional complex Ginzburg–Landau equation, Phys. Rev. E 55 (1997) 5073–5081.
[5] R. Montagne, E. Hernández-Garcia, A. Amengual, M. San Miguel, Wound-up phase turbulence in the complex Ginzburg–Landau equation, Phys. Rev. E 56 (1997) 151–167.
[6] P. Coullet, C. Elphick, L. Gil, J. Lega, Topological defects of wave patterns, Phys. Rev. Lett. 59 (1987) 884–887.
[7] B.I. Shraiman, A. Pumir, W. van Saarloos, P.C. Hohenberg, H. Chaté, M. Holen, Spatiotemporal chaos in the one-dimensional complex Ginzburg–Landau equation, Physica D 57 (1992) 241–248.
[8] M. Howard, M. van Hecke, Hole-defect chaos in the one-dimensional complex Ginzburg–Landau equation, Phys. Rev. E 68 (2003) 026213.
[9] P. Coullet, L. Gil, J. Lega, A form of turbulence associated with defects, Physica D 37 (1989) 91–103.
[10] P. Coullet, L. Gil, J. Lega, Defect-mediated turbulence, Phys. Rev. Lett. 62 (1989) 1619–1622.
[11] S. Zelik, A. Mielke, Multi-pulse evolution, spacetime chaos in dissipative systems, Mem. Amer. Math. Soc. 198 (2009) 1–97.
[12] L. Brusch, M.G. Zimmermann, M. Van Hecke, M. Bar, A. Torcini, Modulated amplitude waves and the transition from phase to defect chaos, Phys. Rev. Lett. 85 (2000) 86–89.
[13] B. Sandstede, A. Scheel, Defects in oscillatory media: toward a classification, SIAM J. Appl. Dyn. Syst. 3 (2004) 1–68.
[14] J.A. Sherratt, M.J. Smith, J.D.M. Rademacher, Patterns of sources and sinks in the complex Ginzburg–Landau equation with zero linear dispersion, SIAM J. Appl. Dyn. Syst. 9 (2010) 883–918.
[15] J.D.M. Rademacher, B. Sandstede, A. Sheel, Computing absolute and essential spectra using continuation, Physica D 229 (2007) 166–183.
[16] B. Sandstede, A. Scheel, Absolute and convective instabilities of waves on unbounded and large bounded domains, Physica D 145 (2000) 233–277.
[17] B. Sandstede, A. Scheel, Gluing unstable fronts and backs together can produce stable pulses, Nonlinearity 13 (2000) 1465–1482.

[18] S.A. Suslov, Numerical aspects of searching convective/absolute instability transition, J. Comput. Phys. 212 (2006) 188–217.
[19] M.J. Smith, J.D.M. Rademacher, J.A. Sherratt, Absolute stability of wavetrains can explain spatiotemporal dynamics in reaction–diffusion systems of lambda–omega type, SIAM J. Appl. Dyn. Syst. 8 (2009) 1136–1159.
[20] J.A. Sherratt, M.J. Smith, Periodic travelling waves in cyclic populations: field studies and reaction–diffusion models, J. Roy. Soc. Interface 5 (2008) 483–505.
[21] J.F.G. Auchmuty, G. Nicolis, Bifurcation analysis of reaction–diffusion equations III, chemical oscillations, Bull. Math. Biol. 38 (1976) 325–350.
[22] J.A. Sherratt, Periodic travelling wave selection by Dirichlet boundary conditions in oscillatory reaction–diffusion systems, SIAM J. Appl. Math. 63 (2003) 1520–1538.
[23] M.J. Smith, J.A. Sherratt, The effects of unequal diffusion coefficients on periodic travelling waves in oscillatory reaction–diffusion systems, Physica D 236 (2007) 90–103.
[24] K. Nozaki, N. Bekki, Pattern selection and spatiotemporal transition to chaos in the Ginzburg–Landau equation, Phys. Rev. Lett. 51 (1983) 2171–2174.
[25] J. Lega, Travelling hole solutions of the complex Ginzburg–Landau equation: a review, Physica D 152 (2001) 269–287.
[26] M.C. Cross, P.C. Hohenberg, Pattern formation outside of equilibrium, Rev. Modern Phys. 65 (1993) 851–1113.
[27] J.A. Sherratt, M.J. Smith, J.D.M. Rademacher, Locating the transition from periodic oscillations to spatiotemporal chaos in the wake of invasion, Proc. Natl. Acad. Sci. USA 106 (2009) 10890–10895.
[28] M.J. Smith, J.A. Sherratt, Propagating fronts in the complex Ginzburg–Landau equation generate fixed-width bands of plane waves, Phys. Rev. E 80 (2009) 046209.
[29] M. van Hecke, Building blocks of spatiotemporal intermittency, Phys. Rev. Lett. 80 (1998) 1896–1899.
[30] L. Gil, Space and time intermittency behaviour of a one-dimensional complex Ginzburg–Landau equation, Nonlinearity 4 (1991) 1213–1222.
[31] H. Chaté, Spatiotemporal intermittency regimes of the one-dimensional complex Ginzburg–Landau equation, Nonlinearity 7 (1994) 185–204.
[32] L. Nana, A.B. Ezersky, I. Mutabazi, Secondary structures in a one-dimensional complex Ginzburg–Landau equation with homogeneous boundary conditions, Proc. Roy. Soc. A 465 (2009) 2251–2265.
[33] R. Deissler, K. Kaneko, Velocity-dependent Lyapunov exponents as a measure of chaos for open-flow systems, Phys. Lett. A 119 (1987) 397–402.
[34] S. Lepri, A. Politi, A. Torcini, Chronotopic Lyapunov analysis II, toward a unified approach, J. Stat. Phys. 88 (1997) 31–45.
[35] G. Giacomelli, R. Hegger, A. Politi, M. Vassalli, Convective Lyapunov exponents and propagation of correlations, Phys. Rev. Lett. 85 (2000) 3616–3619.
[36] J.D.M. Rademacher, Geometric relations of absolute and essential spectra of wave trains, SIAM J. Appl. Dyn. Sys. 5 (2006) 634–649.
[37] L. Brevdo, Convectively unstable wave packets in the Blasius boundary layer, Z. Angew. Math. Mech. 75 (1995) 423–436.
[38] S.M. Tobias, M.R.E. Proctor, E. Knobloch, Convective and absolute instabilities of fluid flows in finite geometry, Physica D 113 (1998) 43–72.
[39] H. Sakaguchi, Instability of the hole solution in the complex Ginzburg–Landau equation, Progr. Theoret. Phys. 85 (1991) 417–421.
[40] H. Chaté, P. Manneville, Stability of the Bekki–Nozaki hole solutions to the one-dimensional complex Ginzburg–Landau equation, Phys. Lett. A 171 (1992) 183–188.
[41] S. Sasa, T. Iwamoto, Stability of phase-singular solutions to the one-dimensional complex Ginzburg–Landau equation, Phys. Lett. A 175 (1993) 289–294.
[42] S. Popp, O. Stiller, I. Aranson, A. Weber, L. Kramer, Localized hole solutions and spatiotemporal chaos in the 1D complex Ginzburg–Landau equation, Phys. Rev. Lett. 70 (1993) 3880–3883.
[43] T. Kapitula, J. Rubin, Existence and stability of standing hole solutions to complex Ginzburg–Landau equations, Nonlinearity 13 (2000) 77–112.
[44] P. Manneville, Dissipative Structures and Weak Turbulence, Academic Press, Boston, 1990.
[45] J. Chomaz, Transition to turbulence in open flows: what linear and fully nonlinear local and global theories tell us, Eur. J. Mech. B 23 (2004) 385.
[46] M. Ipsen, L. Kramer, P. SÃrensen, Amplitude equations for description of chemical reaction–diffusion systems, Phys. Rep. 337 (2000) 193–235.
[47] A. Tsameret, V. Steinberg, Absolute and convective instabilities and noise-sustained structures in the Couette–Taylor system with an axial flow, Phys. Rev. E 49 (1994) 1291–1308.
[48] A. Doelman, Breaking the hidden symmetry in the Ginzburg–Landau equation, Physica D 97 (1996) 398–428.
[49] W. van Saarloos, P.C. Hohenberg, Fronts, pulses, sources and sinks in generalized complex Ginzburg–Landau equations, Physica D 56 (1992) 303–367.
[50] R. Alvarez, M. van Hecke, W. van Saarloos, Sources and sinks separating domains of left-and right-traveling waves: experiment versus amplitude equations, Phys. Rev. E 56 (1997) R1306–R1309.
[51] J.P. Gollub, Order and disorder in fluid motion, Proc. Natl. Acad. Sci. USA 92 (1995) 6705–6711.
[52] D. Barkley, L.S. Tuckerman, Computational study of turbulent laminar patterns in Couette flow, Phys. Rev. Lett. 94 (2005) 14502.
[53] A. Prigent, G. Grégoire, H. Chaté, O. Dauchot, W. van Saarloos, Large-scale finite-wavelength modulation within turbulent shear flows, Phys. Rev. Lett. 89 (2002) 14501.
[54] H. Chaté, P. Manneville, Transition to turbulence via spatio–temporal intermittency, Phys. Rev. Lett. 58 (1987) 112–115.
[55] P. Manneville, Dissipative structures and weak turbulence, Lect. Notes Phys. 457 (1995) 257–272.
[56] H. Chaté, P. Manneville, Role of defects in the transition turbulence via spatiotemporal intermittency, Physica D 37 (1989) 33–41.
[57] H. Willaime, O. Cardoso, P. Tabeling, Spatiotemporal intermittency in lines of vortices, Phys. Rev. E 48 (1993) 288–295.
[58] D. Barkley, L.S. Tuckerman, Mean flow of turbulent-laminar patterns in plane Couette flow, J. Fluid Mech. 576 (2007) 109–137.
[59] D. Moxley, D. Barkley, Distinct large-scale turbulent-laminar states in transitional pipe flow, Proc. Natl. Acad. Sci. USA 107 (2010) 8091–8096.